Heliyon 6 (2020) e03939

Contents lists available at ScienceDirect

Heliyon

journal homepage: www.cell.com/heliyon

Research article

Coupling of chemical, electrochemical and theoretical approach to study the corrosion inhibition of mild steel by new quinoxaline compounds in 1 M HCl

T. Laabaissi [a], F. Benhiba [a,b], M. Missioui [c], Z. Rouifi [a], M. Rbaa [d], H. Oudda [a], Y. Ramli [c], A. Guenbour [b], I. Warad [e], A. Zarrouk [b,*]

[a] Laboratory of Separation Processes, Faculty of Science, University Ibn Tofail, PO Box 133, 14000, Kenitra, Morocco
[b] Laboratory of Materials, Nanotechnology and Environment, Faculty of Sciences, Mohammed V University, P.O. Box. 1014, Agdal-Rabat, Morocco
[c] Laboratory of Medecinal Chemistry, Faculty of Medicine and Pharmacy, Mohammed V University, Rabat, Morocco
[d] Laboratory of Agro-Resources, Polymers and Process Engineering, Department of Chemistry, Faculty of Science, Ibn Tofail University, PO Box 133, 14000, Kenitra, Morocco
[e] Department of Chemistry and Earth Sciences, PO Box 2713, Qatar University, Doha, Qatar

ARTICLE INFO

Keywords:
Electrochemistry
Theoretical chemistry
Quinoxaline derivatives
Mild steel
Corrosion inhibition
SEM/EDX
Simulation dynamics molecular

ABSTRACT

The corrosion inhibition displays of two quinoxaline derivatives, on the corrosion of M-steel (M-steel) in 1 M HCl was studied by gravimetric, electrochemical, scanning electron microscopy (SEM), functional density theory (DFT) and molecular dynamic simulation (MD). The inhibitory efficacy increases with decreasing temperature and increases with inhibitor concentration and reached to 96 % (NSQN) and 92 % (CSQN) at 303 K and the optimum concentration (1×10-3 M). Ultraviolet–visible (UV–vis) spectroscopic analyses confirmed the presence of chemical interactions between the inhibitors and MS surface. The adsorption of NSQN & CSQN on the metallic surface obeys the Langmuir isotherm. A potentiodynamic polarization study confirmed that the inhibitors are of mixed-kind inhibitors. Theoretical computation (DFT) and molecular dynamics simulation (MD) are utilized to understand the mechanism of inhibition.

1. Introduction

Corrosion of metals, particularly M-steel, is in most cases an electrochemical reaction involving the metal and its environment [1]. The M-steel have several utilized, and especially in the fields of industries. One of the most common methods utilized to remove oxides from the surface of M-steel is to clean the metal in an acid bath called "stripping" [2, 3]. While the pickling solution is highly corrosive, we have utilized organic inhibitors (species) which remain an original, practical and less expensive way to ensure adequate protection [4, 5, 6]. These species are added with a small amount to decrease the interaction of environments. The efficiency and the adsorption of the inhibitors are related to their molecular structures, their spatial planarity's, the natures of the functional groups and their attractions. Various chemical compounds of organic or inorganic synthesis are utilized as structures with polar functions of heteroatoms (S, O, N, etc...), heterocyclic electrons and/or π [7, 8], and are considered as responsible for the process adsorption of the compounds. These inhibitors block active corrosion sites on M-steel surface. As you know that the basic molecules of quinoxaline are more utilized in the various fields, namely pharmacology, medicine, agriculture, biology, etc... Likewise, this family is also utilized in the field of corrosion inhibition. The novelty in this work, is evaluating the two organic compounds inhibitory performance against corrosion of M-steel. NSQN & CSQN has been prepared by a simple and effective method with a very good yield. Also, NSQN & CSQN have been characterized by ^{1}H NMR & ^{13}C NMR. This kind of testing of NSQN & CSQN is procured by exploiting polarization and impedance in the electrochemical way [Potentiodynamic Polarization (PDP) & Electrochemical Impedance Spectroscopy (EIS)], these electrochemical techniques have been inspired by gravimetric tests. After the corrosion the surface of the M-steel surface examinations by scanning electron microscopy (SEM) and energy dispersive X-ray spectroscopic supports its inhibition effect (SEM/EDS). The gravimetric solutions have been characterized by UV-Visible spectroscopy (UV-vis). To confirm the experimental tests we carried a theoretical approach by the DFT calculation method and the simulation of the molecular dynamics (MD).

* Corresponding author.
E-mail address: azarrouk@gmail.com (A. Zarrouk).

https://doi.org/10.1016/j.heliyon.2020.e03939
Received 21 November 2019; Received in revised form 2 January 2020; Accepted 4 May 2020

2. Experimental

2.1. Synthesis of styrylquinoxalin

A mixture of 3-methylquinoxalin-2(1H)-one (1) (2 g, 0.0125 mol) and 4-chlorobenzaldehyde (4.2 mL, 0.025 mol) or 4-(dimethylamino)benzaldehyde (3.35 mL, 0.025 mol) were stirred without any solvent for 2 h at 80 °C, after the end of the reaction, a crowded solid precipitate then filtered, dried and from ethanol was crystallized to afford (E)-3-(4-methylstyryl)quinoxalin-2(1*H*)-one (2) and (E)-3-(4-(dimethylamino) styryl)quinoxalin-2(1*H*)-one (3) respectively.

The spectral data results and melting point of (E)-3-(4-chlorostyryl) quinoxalin-2(1H)-one (CSQN):

Yield = 88 %, Mp = 277–279 °C. ^{1}H: δ_{ppm} 8.01–8.06 (d, 1 H, CH $_{ethylene}$, ^{3}J = 15 Hz), 7.64–7.59 (d, 1H, CH $_{ethylene}$, ^{3}J = 15 Hz), 7.29–7.79 (m, 9 ArH), 12.55 (1 H, s, NH); ^{13}C: 139.5 (E $_{ethylene}$), 121.6 (E $_{ethylene}$), 135.3 (C–Cl), 131.64; 132.28; 133.74 (Cq); 115.29, 123.59, 128.59, 128.89, 129.35, 130.01(CH_{Ar}); 154.75(C=$O_{quinoxaline}$); 152.78 (C=N_{amid}).

The spectral data results and melting point of (E)-3-(4-(dimethylamino)styryl) quinoxalin-2(1H)-one are:

Yield = 82 %, Mp = 250–252 °C. ^{1}H: δppm: 3.39 (6 H, s, CH_3); 12.52 (NH, s, 1H); 7.48–7.53 (d, 1 H, CH $_{ethylene}$, ^{3}J = 15 Hz); 7.89–7.94 (d, 1 H, CH $_{ethylene}$, ^{3}J = 15 Hz); 7.30–7.94 (m, 7H_{Ar}); ^{13}C: δppm 37.19 ((CH_3)$_2$); 138.5 (C $_{ethylene}$), 121.6 (C $_{ethylene}$), 151.5 (C–N); 152 (C–N); 145.09; 141.43; 128.21 (Cq); 112.77–124.16 (CH_{Ar}); 157.46(C=$O_{quinoxaline}$); 154.73 (C=N_{amid}).

2.2. Measurement methods for corrosion experiments

Chemical composition materials used for the following gravimetric and electrochemical analyzes by weight (%) is: (0.026 of Si), (0.012 of P), (0.076 of C), (0.192 of Mn), (0.050 of Cr), (0.050 of Ni) (0.135 of Cu), (0.023 of Al), and the balance in iron. 10 mm × 20 mm × 3 mm M-steel surfaces were employed for gravimetric tests, and electrochemical tests. The steel surface approached in an acidic solution for electrochemical tests was 100 mL. The corrosive medium is a solution of molar hydrochloric acid prepared by diluting the concentrated solution to 37%.

2.3. Corrosion analysis

2.3.1. Gravimetric method

The M-steel parts used were carried in 1.0 M HCl in the not including and the including CSQN & NSQN) for 6 h at room temperature [9]. Then the parts were removed, washed with water and acetone and dried in an air oven. From the difference in weights before and after the test, the corrosion rate was determined. The percentage inhibition given is that the intermediary of 3 tests disbursed underneath identical conditions for 10^{-3} M→ 10^{-6} M:

$$E_w(\%) = \frac{w - w_{inh}}{w} \times 100 \quad (1)$$

where the weight loss of these coupons with and without addition of CSQN & NSQN are represented by w_{inh} and w, respectively.

2.3.2. Electrochemical studies

The experimental device used includes an electrolysis cell powered by a potentiostat (Radiometer Analytical PGZ 100), linked to a computer for the acquisition and processing of the results. All electrochemical tests were carried out utilizing a three-electrode cell composed of M-steel as a working electrode, platinum as a counter electrode and saturated calomel electrode (SCE) as a reference electrode, respectively. From in the OCP from the highest frequency (HF) to the lowest frequency (LF) 10×10^4 Hz → 10×10^{-3} Hz, with a root mean square (RMS) amplitude of 10 mV was applied. The electrochemical impedance spectroscopy (EIS) studies have been performed. From a working electrode at a potential range (+250 mV) on OCP at a scanning speed of 0.5 mV/s. The PDP curves were performed.

2.4. Surface characterization: SEM/EDS/UV-Vis

The influence of acid corrosion (1 M HCl) and addition of CSQN & NSQN (10^{-3} M) on morphology and the formed complexes. The surface layer of M-steel coupons were tested by utilizing scanning electron microscopy (SEM) supplied from the JEOL company (Model: JEOL-JSM-IT-100) with attached energy dispersive X-ray unit EDS. UV-Vis [Jenway ultraviolet-visible spectrophotometer (series 67)].

2.5. Theoretical study

2.5.1. DFT methods

The density functional theory (DFT) is a good useful method for explaining the chemical reactivity of a organic compound. In this work, the reactivity of the electronic structures of our compounds were performed utilizing the B3LYP/6-311G (d, p) implemented in Gaussian 09 software package [10, 11, 12]. The corrosion process is carried out in aqueous solutions. It is therefore important to introduce the effect of the solvent in our solutions. Default optimization criteria (Max Force = 0.000015, RMS Force = 0.000010, Max Displacement = 0.00006 and RMS Displacement = 0.000040) were approved. A frequency analysis was performed to make sure that the calculated structures are at a minimum point of the potential energy surface (no imaginary frequency).

The quantum chemical parameters (QCD) associated with energies are the highest occupied molecular orbitals (E_{HOMO}), the lowest unoccupied molecular orbit (E_{LUMO}), and the energy deficit. ($\Delta E = E_{LUMO} - E_{HOMO}$) were calculated. Other chemical indices such as the ionization potential (IP), the electronic affinity (EA), the overall hardness (η) and the electronegativity (χ) are calculated utilizing the equations below:

$$IP = -E_{HOMO} \quad (2)$$

$$EA = -E_{LUMO} \quad (3)$$

$$\eta = \frac{IP - EA}{2} = \frac{E_{LUMO} - E_{HOMO}}{2} = \frac{\Delta E_{gap}}{2} \quad (4)$$

$$\chi = \eta + EA \quad (5)$$

$$\Delta N_{110} = \frac{\varphi - \chi_{inh}}{2(\eta_{Fe_{110}} + \eta_{inh})} = \frac{\varphi - \chi_{inh}}{2\eta_{inh}} \quad (6)$$

The work function value φ is 4.82 eV in the trellis plane (110) of iron [13,14]. While the hardness value of iron (η_{Fe}) is zero for IP = EA which corresponds the metallic bulk.

In addition, the local reactivity of a molecule was performed by Fukui function calculations as follows:

$$f(\vec{r}) = \left(\frac{\partial \rho(\vec{r})}{\partial N}\right)_{V(\vec{r})} \quad (7)$$

where the Fukui works and represents the favorable sites concerning the electrophilic and nucleophilic attacks of inhibitory molecules respectively. Each function is studied as follows:

$$f_i(\vec{r})^+ = q_i(N+1) - q_i(N) \quad (8)$$

$$f_i(\vec{r})^- = q_i(N) - q_i(N-1) \quad (9)$$

The electronic population of the atom k in the neutral, anionic and cationic systems are: q (N), q (N + 1) and q (N - 1) are respectively.

Table 1. The data obtained by the gravimetric study for M-steel/1.0 M HCl/ quinoxaline compounds systems.

Medium	Conc. (M)	w (mg cm^{-2} h^{-1})	E_w (%)
HCl	1.0	3.43 ± 0.20	—
CSQN	10^{-3}	0.22 ± 0.04	93.5
	10^{-4}	0.56 ± 0.02	83.6
	10^{-5}	0.67 ± 0.03	80.4
	10^{-6}	0.94 ± 0.04	72.5
NSQN	10^{-3}	0.14 ± 0.03	95.3
	10^{-4}	0.20 ± 0.02	94.1
	10^{-5}	0.39 ± 0.02	90.0
	10^{-6}	0.43 ± 0.03	87.4

2.5.2. Molecular modeling details

The MD simulations were run utilizing the Studio Materials 8 software. This approach is considerably useful for finding the interaction energies between the inhibitor molecules and the surface (110). In this simulation process, the iron crystal was introduced and split along plane 110 and a slab of 6 Å was used. The Fe (110) surface was relaxed and expanded to a supercell (10 × 10) to provide a large area for inhibitor interaction. A void slab of zero thickness was built [15, 16]. To bring the MD simulation closer to the real system, a supercell with a size of 24.83 × 24.86 × 25.18 Å contains 491 H_2O and one inhibitory molecule was created. The simulations were performed in a simulation box (24.83 × 24.86 × 35.69 Å) via the Discover module implemented in the Materials Studio 8 software with COMPASS force field, a time step of 1 fs, a simulation duration of 200 ps and a NVT set at 303 K, the interactions between Fe (110) and the inhibitor can be understood by interaction and binding energies calculated utilizing the Eqs. (10) and (11):

$$E_{\text{adsorption}} = E_{\text{total}} - \left(E_{\text{surface+solution}} + E_{\text{inhibitor+solution}}\right) + E_{\text{solution}} \quad (10)$$

$$E_{\text{adsorption}} = -E_{binding} \quad (11)$$

where E_{total} is the total energy of the entire system $E_{surface+solution}$ referred to the total energy of Fe (110) surface and solution without the inhibitor and $E_{inhibitor}$ represent the total energy of inhibitor.

3. Results and discussion

3.1. Gravimetric measurement

The samples are immersed in 1 M HCl not including and including of dissimilar concentrations of NSQN & CSQN. The data obtained by the gravimetric study are illustrated by the Table 1.

We noted that for the two compounds, the corrosion rate decreases with the increase in concentration for the two inhibitors, while the inhibitory efficiency increases, and reaches a maximum value of 95.3% at 1×10^{-3} M concentration for NSQN, we notice that the NSQN is more efficient than CSQN. The percentage IE increased with an increase of CSQN and NSQN concentration which is attributed to the inhibitor action by forming an adsorbed protective layer on M-steel surface. It is evident that the adsorption of CSQN and NSQN on the M-steel surface can occur directly by the interaction between heteroatoms/π-electrons of inhibitors/and the vacant orbital of atoms of iron [17]. It seems that the presence of dimethyl attached to as nitrogen atom in the NSQN molecule increases the electron density on the nitrogen atom and enhances the delocalized π electron on the benzene ring, which results in the stronger adsorption of the metal surface, which leads to higher inhibition efficiency of NSQN than CSQN.

3.2. Electrochemical study

3.2.1. Polarization curves

Figure 1 illustrates the potentiodynamic polarization curves of M-steel in 1 M HCl media without and with the addition of NSQN & CSQN at different concentrations at 303 K. Measurements are made in a range of -0.8 V_{SCE} and -0.2 V_{SCE} with a sweep rate of the potential of 0.5 mV s^{-1}, after a prior holding of the working electrode to a stabilization potential during 30 min. The related electrochemical parameters such as corrosion potential (E_{corr}), Tafel cathodic and anodic constants (β_c and β_a respectively) and corrosion current density (i_{corr}) were gathered in Table 2. Corrosion inhibitory efficiency was evaluated from i_{corr} as shown below:

$$E_{pp}(\%) = \frac{i_{corr}^{free} - i_{corr}^{inh}}{i_{corr}^{free}} \times 100 \quad (12)$$

where, i_{corr}^{free} and i_{corr}^{inh} represent, the densities of the corrosion current without and with the presence of quinoxaline NSQN & CSQN compounds.

Based on the above Figure 2 and Table 2, we note that the addition of our organic compounds to the corrosive medium (1 M HCl) induces a general decrease in cathodic and anodic current densities. This effect is more pronounced when the added compound concentration increases.

It turned out from Figure 3 that the addition of NSQN & CSQN in the hydrochloric acid solution results in a clear decrease in the cathodic and anodic current densities, this decrease is all the more marked as the concentration of NSQN & CSQN increases. The analysis of the results recorded in Table 2 has enabled us to conclude that the values of i_{corr} decrease considerably with the increase in the concentration of NSQN & CSQN and the lowest value is observed at a concentration of 1 × 10^{-3} mol L^{-1}, which results in a slowing down of the electrochemical reaction rate due to the formation of a protective inhibitor film on the metal surface via the actives sites present over the metallic surface utilizing their electron-rich centers and form protective films thus creating a barrier between the metal and the corrosive medium [18, 19]. The addition of NSQN & CSQN results in a more or less significant modification of slopes of the lines of the anodic (β_a) and cathodic (β_c) Tafel, this shows that these NSQN & CSQN affects the kinetics of the reduction reaction of the proton and the reaction of the dissolution of M-steel [20, 21]. Examination of the results obtained in Table 2 shows that increasing the concentration of NSQN & CSQN has the effect of displacing the corrosion potential (E_{corr}). In the literature [18, 21], if the displacement of the corrosion potential is more than 0.085 V compared to the blank,

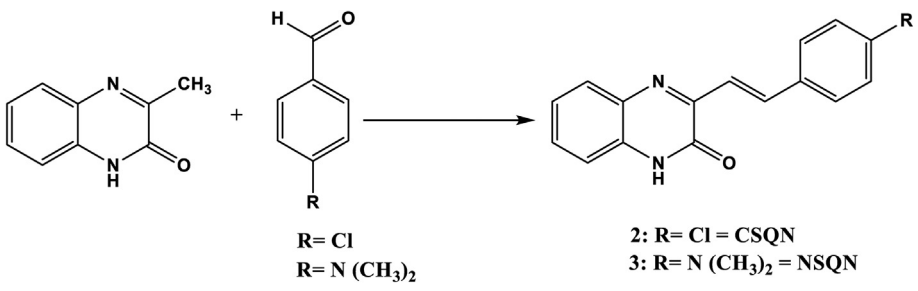

Figure 1. Molecular structures of (E)-3-(4-(dimethylamino) quinoxalin-2(1*H*)-one (NSQN) and E)-3-(4chlorostyryl)quinoxalin-2(1*H*)-one (CSQN).

Table 2. Inhibitory efficacy and electrochemical parameters of 1 M HCl corrosion of M-steel without and with addition of different concentrations of NSQN & CSQN at 303 K.

Medium	Conc. (M)	E_{corr} (mV vs. SCE)	i (μA cm^{-2})	Tafel slopes (mV dec^{-1})		E_{pp} (%)
				β_c	β_a	
HCl	1.0	-470.8 ± 0.3	556.5 ± 0.6	-109.6	67.8	—
CSQN	10^{-3}	-424.8 ± 0.5	049.9 ± 0.4	-99.2	67.3	91.1
	10^{-4}	-402.1 ± 0.6	085.6 ± 0.5	-146.1	64.3	84.6
	10^{-5}	-399.2 ± 0.4	135.1 ± 0.5	-88.8	54.7	75.7
	10^{-6}	-420.1 ± 0.8	195.8 ± 0.4	-77.8	64.5	65.0
NSQN	10^{-3}	-410.5 ± 0.9	030.4 ± 0.2	-128.5	76.5	94.5
	10^{-4}	-410.3 ± 0.9	047.2 ± 0.3	-101.7	65.8	91.5
	10^{-5}	-408.3 ± 0.4	057.9 ± 0.1	-108.1	85.2	89.6
	10^{-6}	-418.2 ± 0.2	131.7 ± 0.3	-67.9	88.4	76.2

the inhibitor can be classified as anodic or cathodic type, if not, it is of mixed type. For our case this displacement is of the order of 0.056 V for (NSQN) and 0.0507 mV for (CSQN) towards the anodic zone which indicates that these NSQN & CSQN are of mixed types.

From the table above, we notice that the corrosion densities (i_{corr}) decrease sharply. The corrosion current density is reduced from 556.5 μA/cm^2 for relieving in the absence of inhibitor to 49.9 μA/cm^2 and 30.4 μA/cm^2 for NSQN & CSQN, respectively. These observations confirm the mixed nature of the inhibitors tested and clearly show that these inhibitors reduce the anodic dissolution rate of steel and the H^+ proton reduction rate [20].

3.2.2. Impedance spectroscopy

According to the Figure 3, the Nyquist diagrams presenting a single loop form a semicircle. This result shows that the corrosion process was controlled by a charge transfer reaction. This is consistent with the observation of Bode and phase plots diagrams (Figure 4). These spectra were recorded at the stabilization potential after 30 min immersion at 303 K [22]. The strength of this technique is to differentiate the reaction phenomena by their relaxation time. The impedance loop depression has been interpreted in the literature by a distribution of time constants derived from the heterogeneity of the surface [23]. This Heterogeneity results from the irregular distribution of surface properties of the electrode or the random adsorption of inhibitors on the surface of M-steel [24, 25]. The impedance diagrams recorded in the presence of the NSQN & CSQN inhibitors show a single capacitive loop in the studied frequency domain for all concentrations. In addition, the size of the impedance loops increases with the increasing concentration of studied inhibitors, indicating that the inhibition efficiency is proportional to the inhibitors. This reflects the increase in the area covered by the inhibitory molecules together with the increase in inhibitor content. The flattened shape of the capacitive loops and the phase shift with respect to the real axis testify to the non-ideal behavior of the studied systems expressed in terms of CPE in the equivalent electrical circuit (see Figure 5).

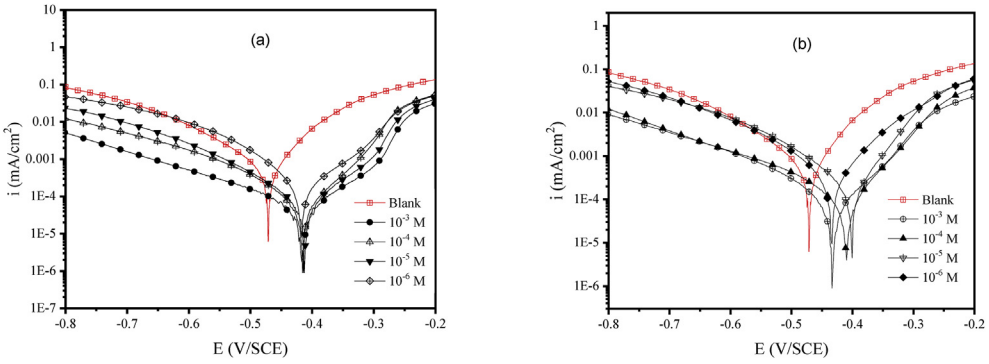

Figure 2. Polarization curves for M-steel/1 M HCl/NSQN (a) and CSQN (b) systems at 303 K.

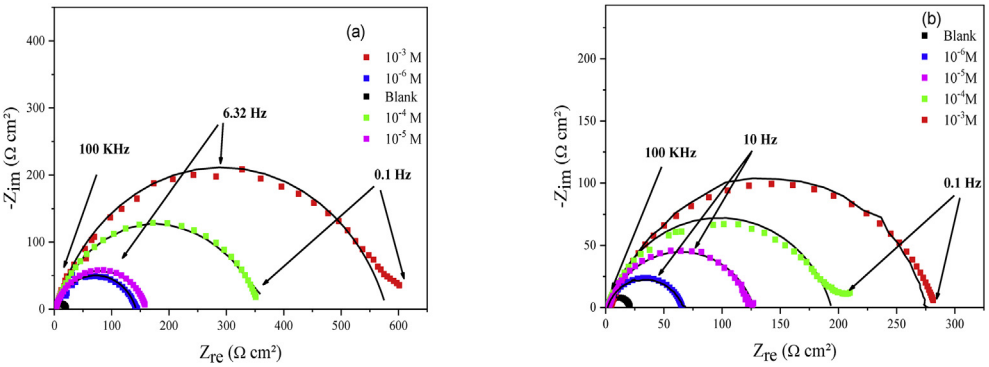

Figure 3. Impedance diagrams for M-steel/1 M HCl/NSQN (a) and CSQN (b) systems at 303 K.

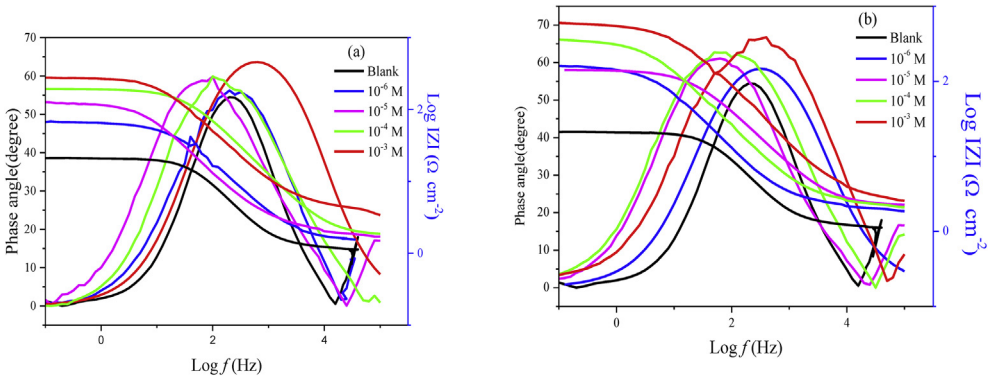

Figure 4. Bode diagrams for M-steel/1 M HCl/NSQN(a) and CSQN(b) systems at 303 K.

Figure 5. EEC at electrochemical interface: M-steel/1 M HCl + (NSQN & CSQN).

To accurately simulate the electrode-electrolyte interface in such situations, it is compatible to use a constant-phase element (CPE) instead of a pure double-layer capacitor and its impedance can be given by:

$$Z_{CPE} = Q^{-1}(i\omega)^{-n} \tag{13}$$

where Q named the CPE constant, n is a CPE exponent determining the phase shift which can be utilized as a gauge of roughness or heterogeneity of the surface ($0 \prec n \prec 1$), $i^2 = -1$ defined as an imaginary number and ω is the angular frequency ($\omega = 2\pi f$, where f is the frequency). The values of n vary with respect to the blank solution and decrease for NSQN & CSQN, this decrease is attributed to the growth in the heterogeneity of the initial surface of M-steel electrode, the CPE can be considered as a pseudo-capacitor [26]. The values from the parametric adjustment of the experimental impedance spectra using the proposed equivalent electrical circuit (Figure 4) have been calculated and summarized in the Table 3.

From Table 3, we see that the C_{dl} values decrease with increasing concentration of CSQN and NSQN. As the R_P values increase. It is also mentioned that the highest R_P values obtained are associated with a slower corrosion system, due to a decrease in the active surface required for the corrosion reaction [27, 28]. This indicates that quinoxaline compounds (CSQN and NSQN) effectively inhibit the corrosion reaction.

These values also reflect the degree of difficulty of the corrosion reaction, and more than its value is high, more than its corrosion rate is low. The highest R_p (279 Ω cm^2 for CSQN) and (577 Ω cm^2 for NSQN) have been obtained at 1×10^{-3} M. It is also noted that at the same table as, at the same concentration inhibitor, the value of R_p is in accordance with the following order NSQN > CSQN. In addition, the Q values in the presence of CSQN and NSQN are lower compared to the uninhibited system. This can be assigned to the displacement of H_2O molecules by inhibitory molecules at the metal/solution interface leading to the formation of a protective layer on the surface of the M-steel [29].

The addition of CSQN and NSQN minimizes the inhomogeneity coefficient values (n) relative to blank, which explains the steel surface is relatively more heterogeneous and it probably due to a non-uniform adsorption of organic compounds on the M-steel. The NSQN compounds and CSQN adsorb to the surface of M-steel and block available sites for corrosive dissolution resulting in increased values correlated with corrosion inhibition performance the bias resistor (R_p) can be used to calculate the inhibition efficiency shown below [30]:

$$E(\%) = \frac{R_{p(inh)} - R_p}{R_{p(inh)}} \times 100 \tag{13a}$$

where the terms R_p and $R_{p(inh)}$ designates the polarization resistance without and with the NSQN and the CSQN respectively. The values of the double layer capacitance (C_{dl}) can be estimated as given below [29]:

$$C_{dl} = Y_0(\omega_{max})^{n-1} \tag{14}$$

where ω_{max} symbolizes the frequency at which the imaginary quantity of impedance reached the maximum value (rad s^{-1}).

EIS measurements also confirm the inhibiting nature of our both inhibitors, and the E (%) values obtained from this method show the almost trend as those obtained from the polarization technique and weight loss method. The use of the quinoxaline derivatives as corrosion inhibitors have been widely reported by several authors [31, 32, 33, 34]. As an example,

Table 4 reports the percentage inhibition efficiency for some selected quinoxaline derivatives used as corrosion inhibitors in 1 M HCl medium. The values of inhibition efficiency, given in this table, were obtained utilizing EIS measurement after 1/2 h of immersion in 1 M HCl solution containing 10^{-3} M of quinoxaline derivative at 303 K. By comparing these data, we can show that our quinoxaline derivative (NSQN) is the

Table 3. EIS parameters for M-steel/1 M HCl/NSQN & CSQN systems at 303 K.

Medium	CoConc. (M)	R_p (Ω cm^2)	n	Q×10^4 (S^n Ω^{-1} cm^{-2})	C_{dl} (μF/cm^2)	ERp (%)	θ
Blank	1	20.5 ± 0.05	0.900 ± 0.06	2.061 ± 0.580	104.8	—	—
NSQN	10^{-3}	5770 ± 0.8	0.810 ± 0.07	0.619 ± 0.020	28.3	96.4	0.964
	10^{-4}	356 ± 0.6	0.790 ± 0.06	0.882 ± 0.058	35.5	94.2	0.942
	10^{-5}	158 ± 0.4	0.760 ± 0.05	1.491 ± 0.169	46.1	87.3	0.873
	10^{-6}	140 ± 0.7	0.740 ± 0.09	1.670 ± 0.120	47.7	85.0	0.850
CSQN	10^{-3}	279 ± 0.7	0.790 ± 0.08	0.991 ± 0.420	38.2	92.8	0.928
	10^{-4}	192 ± 0.5	0.782 ± 0.09	0.999 ± 0.231	39.6	89.3	0.893
	10^{-5}	125 ± 0.6	0.771 ± 0.05	1.359 ± 0.011	40.2	83.6	0.836
	10^{-6}	64.0 ± 0.8	0.774 ± 0.04	1.987 ± 0.411	53.9	67.9	0.679

Table 4. Percentage inhibition efficiency for different quinoxaline derivatives in 1 M HCl (the concentration used is 10^{-3} M).

Quinoxaline derivative	Highest inhibition efficiency (%)[a]	Metal exposed	Reference
(E)-3-(4-methoxystyryl)-7-methylquinoxalin-2(1H)-one	87.0	Mild steel	[31]
2-(4-methoxyphenyl)-7-methylthieno [3,2-b] quinoxaline	94.0	Mild steel	[31]
6-methylquinoxaline-2,3(1H,4H)-dione	92.6	Carbon steel	[32]
2-(8-hydroxyquinoxalin-5-yl)acetonitrile	91.0	Carbon steel	[33]
(E)-3-(4-methylstyryl)quinoxalin-2(1H)-one	91.1	Mild steel	[34]
(E)-3-(4chlorostyryl)quinoxalin-2(1H)-one	92.8	Mild steel	This work
(E)-3-(4-(dimethylamino)quinoxalin-2(1H)-one	96.4	Mild steel	This work

[a] The inhibition efficiency values were determined utilizing EIS measurements at 303 K after 1/2h of immersion.

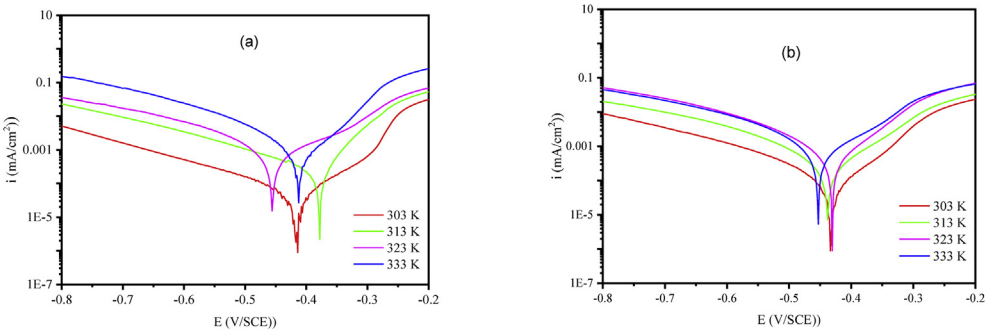

Figure 6. Polarization curves of M-steel/1 M HCl with the addition of 1×10^{-3} M NSQN (a) and CSQN (b) at different temperatures.

best effective inhibitor in 1 M HCl. Moreover, we get a high value of efficiency even at a lower concentration of this quinoxaline derivative (85.0% at 10^{-6} M of PDQO).

3.3. Temperature effect

The effect of temperature is mandatory in the study of corrosion of steel in order to know the behavior of high-temperature inhibitors. In order to know how this factor can influence the inhibitory efficacy of NSQN & CSQN, we have varied the temperature between 303 and 333 K with a pitch of 10 K. In this context, stationary electrochemical measurements of M-steel with and without the addition of NSQN & CSQN at a concentration of 1×10^{-3} M were performed.

3.3.1. Potentiodynamic polarization curve

The Tafel curves of M-steel in 1 M HCl without and with addition of NSQN and 1×10^{-3} M CSQN are summarized in the Figures 6 and 7. While Table 5 gathers the different electrochemical parameters associated with these curves i = f (E).

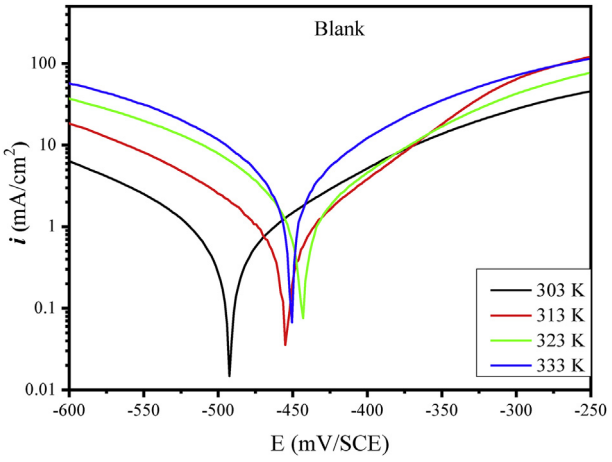

Figure 7. Polarization curves of M-steel/1 M HCl at different temperatures.

The results in Table 5 show that the percentage of E_{PP}(%) implies a downward trend, the rise in temperature shows that the inhibitor molecules desorb from the surface of M-steel. Temperature growth also increases the dissolution rate of the metal, resulting in an increased corrosion rate (i_{corr}) and a concomitant decrease in corrosion protection. It also shows that NSQN & CSQN retain their inhibitory properties for all temperatures studied. However, in the case of the inhibitor NSQN, which proved to be the best inhibitor of this family, the decrease in the inhibitory performance is less important and reaches 55 % at 333 K.

3.3.2. Thermodynamic activation parameters

The dependence between the corrosion current density (i_{corr}) and the temperature allows us to calculate the value of the activation dependencies between the corrosion current and the time of calculation of the energy value of the corrosion process, at different temperatures, with and without of compounds NSQN & CSQN, according to the Arrhenius equation:

$$i_{corr} = k\exp\left(\frac{-E_a}{RT}\right) \tag{14a}$$

E_a is the activation energy, R is the perfect gas constant, k is a pre-exponential factor, T is the absolute temperature and i_{corr} is the density of the corrosion current. The plot of Ln (i_{corr}) = f (1/T) in the absence and in the presence of quinoxalines (Figure 8), was performed in order to calculate the activation energy from the Arrhenius relation [35]. Entropy ΔS_a were calculated utilizing the following equation:

$$i_{corr} = \frac{RT}{Nh}\exp\left(\frac{\Delta S_a}{R}\right)\exp\left(\frac{\Delta H_a}{RT}\right) \tag{15}$$

We have calculated the values of ΔH_a and ΔS_a (Figure 8 and Table 6). Thanks to the straight lines obtained have a slope equal to ($-\Delta H_a/R$) and an ordinate at the origin equal to [Ln (R/Nh) + (ΔS_a/R)].

The activation energy value E_a of the hydrogen evolution reaction in HCl medium in the nonexistence of CSQN & NSQN (45.14 kJ/mol) is in accordance with the values given in the literature for M-steel in the same acid medium. The addition of CSQN & NSQN to the corrosive solution is accompanied by an augment in E_a; this could be attributed to the

Table 5. Corrosion rate and inhibitory efficacy of NSQN & CSQN at a concentration of 1×10^{-3} M as a function of temperature for M-steel in 1.0 M HCl.

Medium	T (K)	-E_{corr} (mV/SCE)	i_{corr} (μA cm^{-2})	Tafel slopes (mV dec^{-1})		E_{PP}(%)
				β_c	β_a	
Blank	303	-496.0	556	-105.0	55.4	—
	313	-454.0	860	-80.0	69.0	—
	323	-443.0	1840	-87.0	96.0	—
	333	-450.0	2600	-86.7	106.9	—
NSQN	303	-410.5	30	-128.5	76.5	94.0
	313	-383.4	198	-188.4	57.0	76.9
	323	-460.0	677	-233.1	155.0	62.5
	333	-417.0	1159	-179.1	89.3	55.4
CSQN	303	-424.8	50	-99.2	67.3	91.0
	313	-442.2	239	-170.8	112.7	72.2
	323	-435.0	811	-186.0	111.3	55.9
	333	-457.6	1376	-232.2	114.5	47.0

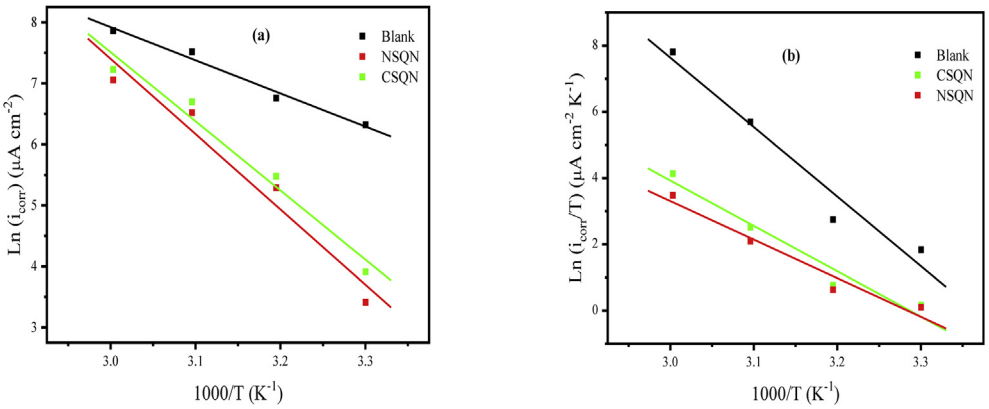

Figure 8. Variation in Ln i_{corr} as a function of 1/T (a) and Ln i_{corr}/T as a function of 1/T (b) of steel in 1M HCl without and with the addition of NSQN & CSQN at 1×10^{-3} M.

presence of an energy barrier for the corrosion reaction due to the existence of cations of the metal/electrolyte interphase inhibitor, which shows a change in the mechanism of passage of metal in solution [9]. The positive values of ΔH_a mean that the dissolution reaction is an endothermic process [36]. Relatively lower values of ΔH_a than that of E_a values ($E_a > \Delta H_a$) indicate that results derived in the present study is consistent with the thermodynamic relationship ($E_a - \Delta H_a = RT$) [36]. The activation entropy ΔS_a changes the sign, and becomes positive, this reflects an increase in molecular disorder after the addition of CSQN & NSQN [37]. We can notice that E_a and ΔH_a vary in the same way, moreover, the average value of the difference $E_a - \Delta H_a$ is approximately 2.58 kJ/mol very close to the average value of the product RT, where T is between 303 and 3333 K, this is explained by the fact that the corrosion process is a unimolecular reaction, characterized by the equation: $E_a - \Delta H_a = RT$.

3.4. Adsorption isotherm

To determine the type of adsorption performed between an inhibitor and the M-steel surface, we used the adsorption isotherm method. In fact, in aqueous solution, the adsorption at the solution metal interface of organic molecules coming from the solution is generally accompanied by the desorption of H_2O-molecules already adsorbed on the metal surface. This adsorption is therefore considered as a substitutional adsorption phenomenon [38] as shown by the following reaction:

$$Org_{aq} + xH_2O_{ads} \rightarrow Org_{ads} + xH_2O_{aq} \quad (16)$$

x it is the number of H_2O-molecules replaced by the studied molecule.

Table 6. Activation parameters of 1 M HCl steel without and with the addition of 1×10^{-3} M NSQN & CSQN.

Medium	E_a (kJ mol^{-1})	ΔH_a (kJ mol^{-1})	ΔS_a (J mol^{-1}K^{-1})
Blank	45.14	42.56	-52.29
NSQN	102.59	99.93	115.56
CSQN	94.19	113.81	176.75

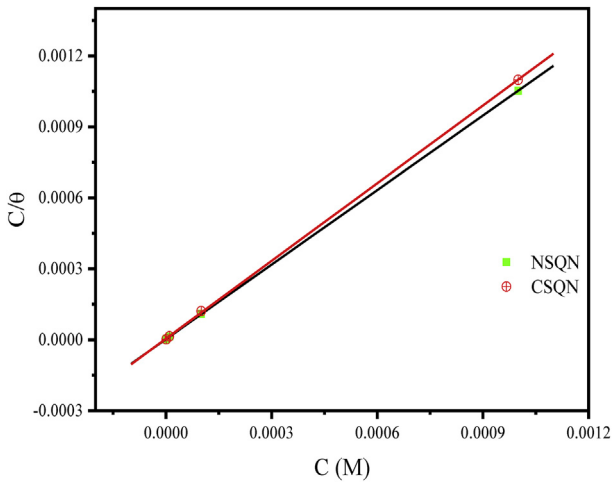

Figure 9. Langmuir adsorption curve of NSQN & CSQN at 303 K.

Table 7. Thermodynamic adsorption characteristics of NSQN & CSQN on the M-steel surface in 1M HCl medium.

Inhibitors	Linear regression coefficient	Slopes	K_{ads} (L/mol)	ΔG°_{ads}(kJ/mol)
NSQN	0.9999	1.09	399649	-42.61
CSQN	0.9998	1.07	205971	-40.93

Results experimentally have been adjusted to diverse isotherms among which the Langmuir isotherm has provided the best fit and can be represented as follows [29]:

$$C / \theta = 1/K_{ads} + C \quad (17)$$

where C denotes the concentration of NSQN & CSQN in M, θ symbolizes surface coverage (Table 3), and K_{ads} represents the equilibrium constant of adsorption. The Langmuir isotherm for adsorption of NSQN & CSQN are shown in Figure 9.

We can determine ΔG°_{ads} by means of the following relation [8]:

$$K_{ads} = \left(\frac{1}{55.5}\right)\exp\left[-\frac{\Delta G^{\circ}_{ads}}{RT}\right] \quad (18)$$

where (55.5) M is the concentration of water in the solution, R the constant of perfect gases. The electrochemical thermodynamic parameters listed in Table 7. The Langmuir model appears to be the most adequate for describing the adsorption of the quinoxaline compounds studied on the surface of the steel. This is confirmed by the slope and coefficient values linear regression close to the unit.

By and large, the great value of K_{ads} shows that the two salts is readily and highly adsorbed on the metal surface, prompting superior protection efficiency. For our situation, the substantial interaction of quinoxalin-2(1*H*)-one derivative with steel can be credited to the existence of heteroatoms, for example, *O, N* and π electrons in the quinoxaline compounds. According to Table 8, the existing values of K_{ads} follow the order: K_{ads} (NSQN) > K_{ads}(CSQN), suggesting that the NSQN show top protection performance than the other derivative.

We can say we have physical adsorption if $\Delta G^{\circ}_{ads} \leq$ -20 kJ/mol and the chemical adsorption if $\Delta G^{\circ}_{ads} \geq$ -40 kJ/mol. Calculated free energy values are around -40 kJ/mol, which implies that adsorption of NSQN & CSQN inhibitors involve chemisorption.

3.5. Surface analysis

3.5.1. SEM study

To complement the results obtained by gravimetric (weight loss) and electrochemical (PPD, EIS) measurements. Surface analysis utilizing the scanning electron microscopes (SEM) was performed for secondary electron imaging observation, according to the topography of the sample. SEM images of the M-steel surface after immersion in 1 M HCl without and in the presence of the optimal concentration of NSQN & CSQN (1×10^{-3} M) are presented in Figure 10.

After immersing in an uninhibited solution, the high-resolution SEM micrograph (Figure 10-b) shows that the surface of the M-steel was severely damaged due to a rapid corrosion attack in the absence of the inhibitor. However, in the presence of NSQN & CSQN a relatively smooth and less corroded steel surface morphology can be observed (Figure 10b and c). This shows the formation of a protective layer of two quinoxalinic compounds on the surface of the steel. The corrosion inhibition of M-steel in 1 M HCl utilizing inhibitory molecules can be explained by the strong tendency of the latter to stick to the steel surface [39,40]. The high inhibitory performance of studied compounds suggests a strong binding of the NSQN & CSQN molecules to the metal surface due to the presence of free electron pairs, heteroatoms and π orbitals, resulting in blocking of active sites and consequently the reduction of the rate of corrosion.

Table 8. Different values of QCD of neutral and protonated molecules.

Inhibitors	NSQN		CSQN	
Formes	Neutral	Protonated	Neutral	Protonated
Descriptors				
E_{HOMO} (eV)	-4.996	-5.688	-5.820	-6.572
E_{LUMO} (eV)	-2.473	-3.810	-2.198	-3.340
ΔE_{gap} (eV)	2.523	1.878	3.622	3.232
(χ (eV)	3.7345	4.749	4.009	4.956
(η (eV)	1.2615	0.939	1.811	1.616
ΔN_{110}	0.430	0.038	0.224	-0.042

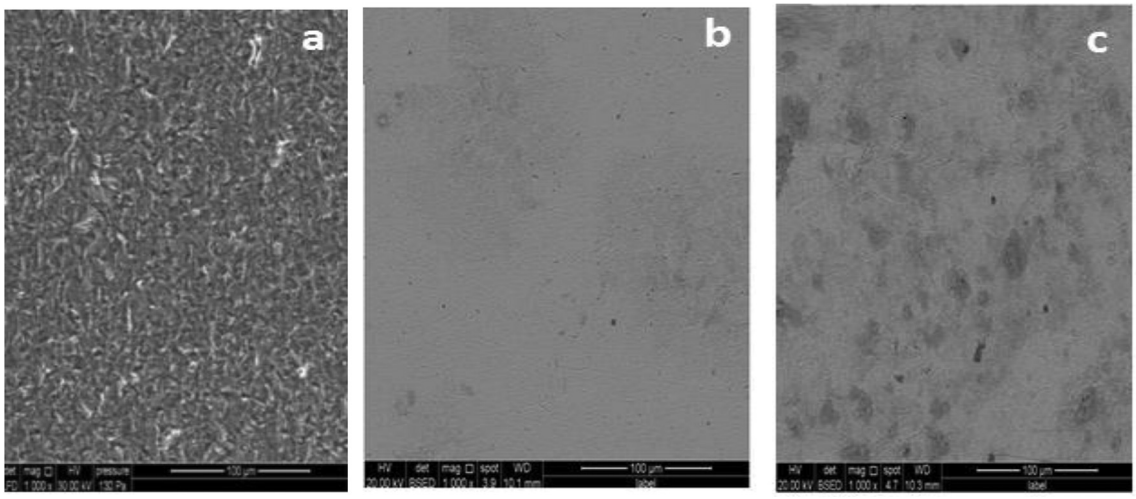

Figure 10. SEM images of the surface condition of M-steel: after immersion for 6 h: 1 M HCl (a), 1 M HCl +1×10^{-3} M NSQN (b), 1 M HCl +1×10^{-3} M CSQN (c).

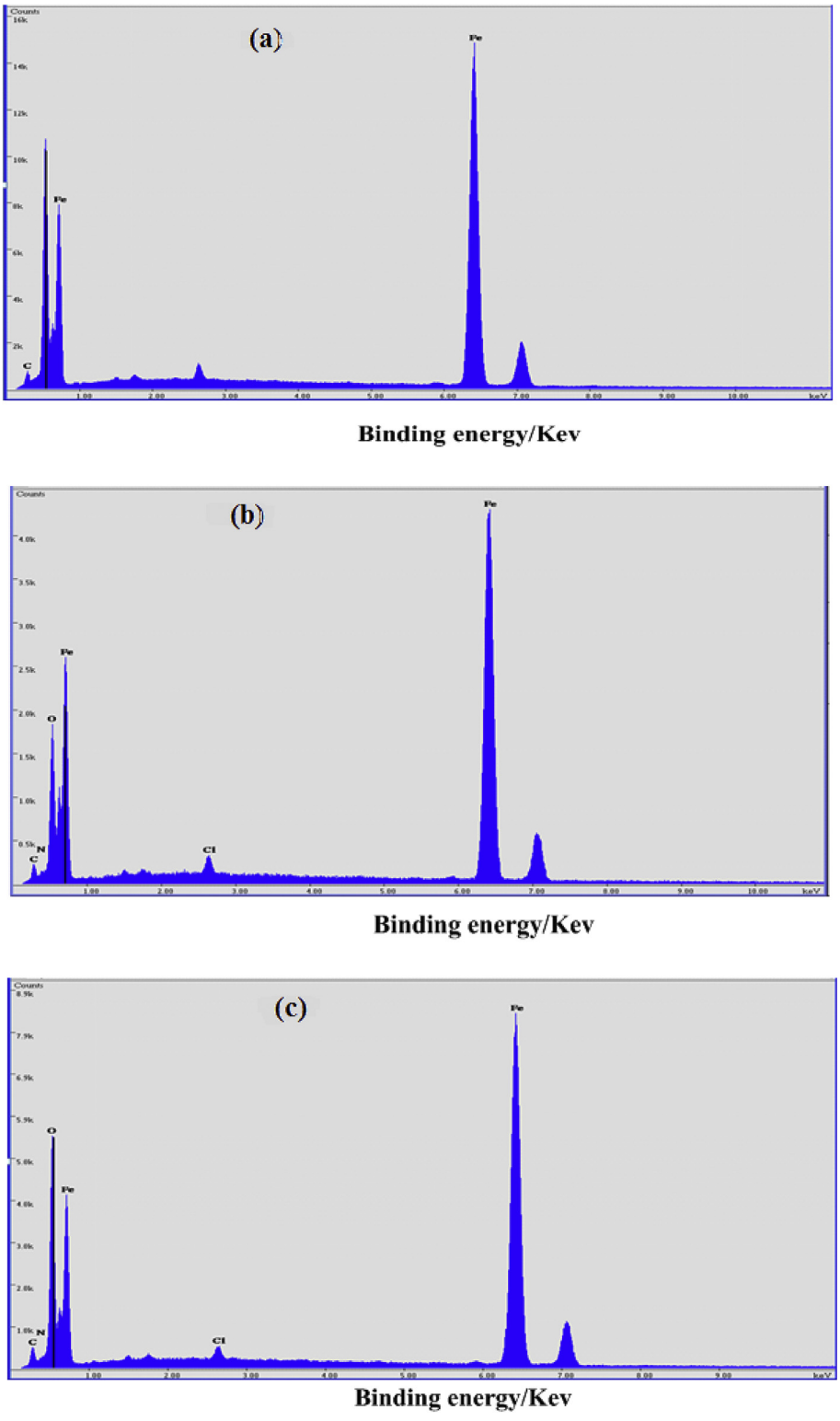

Figure 11. Qualitative EDS of surface condition after 6 h of immersion in the aggressive solution alone (HCl (1 M)) (Blank) (a), 1 M HCl $+1\times10^{-3}$ M NSQN (b), 1 M HCl $+1\times10^{-3}$ M CSQN (c).

3.5.2. X-ray energy dispersion (EDS)

The EDS spectra of the surface of M-steel is illustrated also in Figure 11.

The EDS spectrum reported in Figure 11 shows the characteristic peaks of the sample and a marked presence of Fe, O and C atoms in the nonexistence and in the existence of the NSQN & CSQN inhibitor, and shows a small peak of oxygen and iron relative to the uninhibited solution, reflecting a decrease in the proportion of iron oxide on the metal surface. This result confirms the formation of the protective inhibitor film [41]. With these results, we confirmed that the high inhibitory efficiency values obtained in weight loss and electrochemical measurements can be attributed to a good protective film formation on the surface of the M-steel substrate.

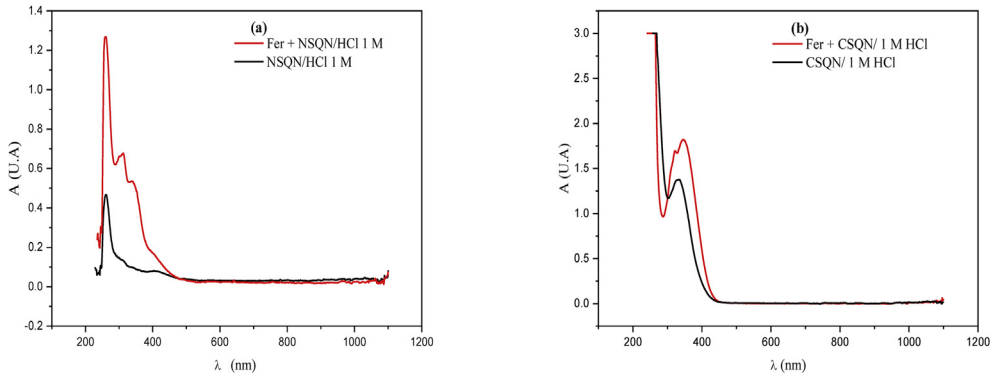

Figure 12. UV-visible spectra of the 1 M HCl solution in the presence of 1×10^{-3} M NSQN (a) inhibitors and CSQN (b) before immersion (black) and after 24 h immersion in M-steel (red).

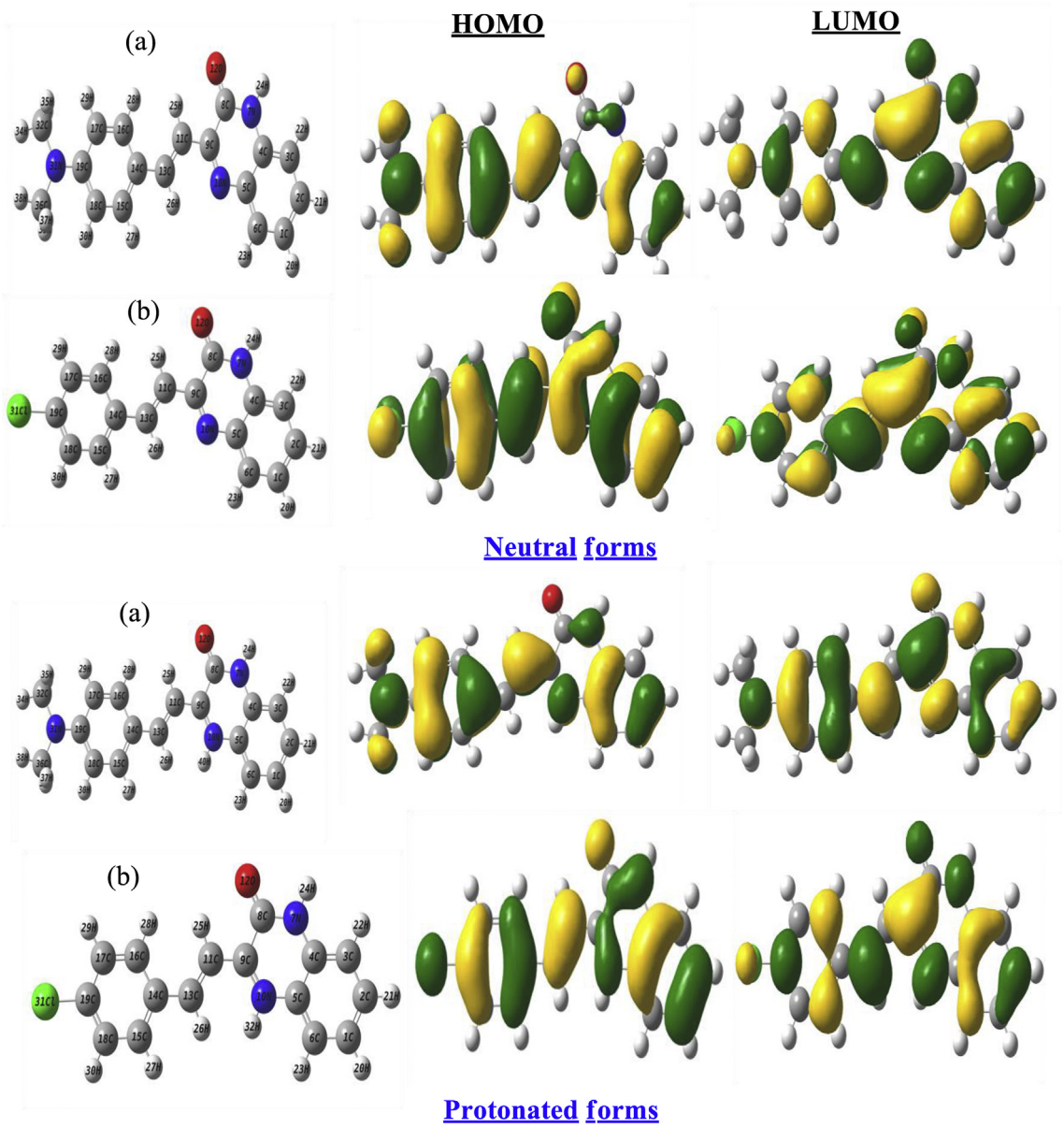

Figure 13. Optimized structures and electron density distribution of FMOs (HOMO and LUMO) of neutral and protonated molecules (NSQN (a) and CSQN(b)).

3.5.3. UV-Vis spectroscopy

In order to prove the possibility of formation of complex (inhibitor-Fe), the UV-visible absorption spectra obtained from a 1 M HCl solution containing 1×10^{-3} M NSQN & CSQN before and after 24 h of immersion 303 K M-steel is shown in Figure 12. Earlier work has reported that displacement of wavelength with variation in absorbance indicates the formation of a complex between the two species in solution.

The absorption spectra of NSQN before the immersion of M-steel have absorption bands between 300.51-320.42 nm and are almost identical and can be ascribed to the π - π * electronic transitions of the aromatic ring. It is noted that there is a displacement of the absorbance of these bands without there being a very remarkable difference in the appearance of the spectra before and after the submersion of NSQN & CSQN inhibitors indicating a possibility of interaction between our NSQN & CSQN inhibitors and M-steel. These experimental findings demonstrate the possibility of complex formation between the Fe^{2+} cation and NSQN & CSQN in HCl (between the two species in solution) [25].

3.6. Overview of quinoxaline reactivity behavior by DFT and MD simulation

The objective of this section is to study the global and local reactivity of NSQN & CSQN in the neutral and protonated forms of the quinoxaline family in the liquid aqueous phase (Solvent effect (H_2O)). In this sense, driven by the successful application of theoretical calculations in the search for corrosion inhibitor, an attempt is made to elucidate the mechanism of inhibition of the NSQN & CSQN and to give an appropriate explanation to the experimental results utilizing the DFT and MD simulation, which are very suitable methods for acquiring new insights into the mechanism of inhibition [42].

3.6.1. Study of the correlation between molecular structure and inhibitory activity via DFT

3.6.1.1. Optimized structures and FMOs distribution of neutral and protonated inhibitors CSQN and NSQN. The polarizable continuum model (PCM) has been used in which the solute is considered to be a molecule trapped in a cavity surrounded by the solvent [43,44]. The quantum chemical descriptors (QCD) were calculated in the neutral and the protonated state in the presence of water with the dielectric constant $\varepsilon_r = 78.39$. In order to characterize the mechanism of attack of NSQN & CSQN in the hydrochloric acid medium, we are interested in studying our NSQN & CSQN protonated and not protonated in the aqueous phase, on the one hand, we have studied the solvent effect (H_2O), and on the other hand, we interpreted protonation effect. In this context, Figure 13 represents the optimized structures and the electron density distribution of the FMOs of the loaded and uncharged NSQN & CSQN which predicts the distribution of the spatial electronic densities of these orbital's on which type of atoms are the majority and to deduce their reactivity. The optimal geometrical configuration of the molecules shows us that they are almost all flat. This suggests that NSQN & CSQN have an almost parallel arrangement on the surface of M-steel. Thus, the difference in the inhibition of the efficiency of the two inhibitors cannot be explained in terms of their geometric configuration. It could be explained in terms of the energies of FMOs and other quantum chemistry indices of NSQN & CSQN (See Table 8). The nearly uniform density distribution of the FMOs shown in Figure 13 shows that adsorption is likely to occur at multiple reactive sites distributed along the molecular structure, which may increase adsorption stability and lead to the improvement of the efficacy of NSQN & CSQN.

3.6.1.2. Main global descriptors derived from the conceptual DFT of protonated and neutral inhibitors. Quantitative chemical descriptors are listed in Table 8, after analyzing the data from this table, it is clear that the values of ΔE are classified in the following order: NSQN < CSQN, this ranking is valid for both studied forms, which means that the NSQN molecule is easy to adsorb to the metal surface and increases its inhibitory efficiency [45, 46]. A higher value of η and a low value of χ mean better inhibitory performance and imply greater polarizability. The comparison between the values of η and x shows that NSQN & CSQN can react easily with M-steel surface. It's made NSQN has a good reactivity with the electrode surface thanks to the increase in the value of the

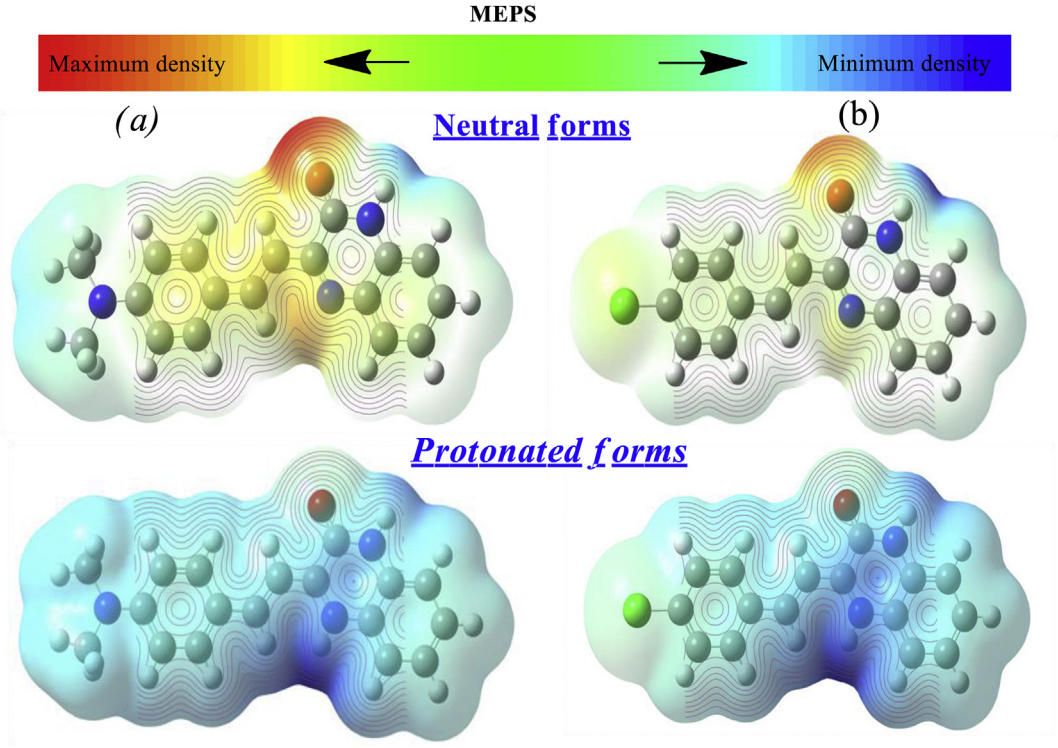

Figure 14. Representations of the protonated and unprotonated molecular electrostatic potential with the electrostatic contour of (a) NSQN and (b) CSQN.

Table 9. Different values of Mulliken loads and Fukui indices of neutral and protonated inhibitory molecules.

Inhibitors	NSQN		CSQN	
Forms	Neutral	Protonated	Neutral	Protonated
Atoms				
C1	-0.039	-0.051	-0.044	-0.059
C2	-0.022	-0.058	-0.024	-0.048
C3	-0.113	-0.096	-0.113	-0.089
C4	0.251	0.219	0.249	0.225
C5	0.184	0.111	0.171	0.201
C6	-0.095	-0.090	-0.086	-0.075
N7	-0.240	-0.222	-0.230	-0.300
C8	0.391	0.445	0.394	0.442
C9	0.129	0.169	0.112	0.179
N10	-0.332	-0.206	-0.293	-0.249
C11	-0.126	-0.105	-0.098	-0.074
O12	-0.544	-0.308	-0.529	-0.483
C13	-0.008	-0.039	-0.011	-0.019
C14	0.173	-0.053	0.197	0.065
C15	-0.069	-0.047	-0.061	-0.042
C16	-0.099	-0.080	-0.088	-0.070
C17	-0.115	-0.099	-0.060	-0.034
C18	-0.121	-0.107	-0.061	-0.037
C19	0.293	0.261	0.194	-0.001
N31	-0.246	-0.283	—	—
C32	-0.002	-0.006	—	—
C36	-0.002	-0.005	—	—
C31	—	—	—	—
Cl 31	—	—	-0.207	-0.060
TNC	-2.173	-1.983	-1.905	-1.640

electronegativity (χ(neutral) = 3.7345 eV; χ (protonated) = 4.749 eV) and the reduction of hardness electronegativity (χ(neutral) = 1.2615 eV; χ (protonated) = 0.939 eV). These results show that after protonation the structural reactivity increases.

About the evolution of the number of electrons transferred ΔN, according to Elnga et al. [47], the inhibition efficiency increases with the capacity of the molecule to give electrons to the surface of the metal if and only if the value of ΔN is inferior to 3.6. It can be concluded from Table 8 that all values of ΔN are positive and inferior to 3.6 indicate that molecules can give electrons to the iron surface through the formation of coordination bonds [48]. Table 8 indicates that the power to give the electrons of our neutral compounds is ranked in the following order: ΔN_{110} (NSQN) = 0.430 > ΔN_{110} (CSQN) = 0.224. From Table 8, it can be seen that after the protonation of NSQN & CSQN the calculated ΔN_{110} value are decreased, but remaining positive for NSQN, this result shows that this protonated molecule is still able to release the electrons on the surface of the metal. While the calculated value of ΔN_{110} for CSQN has been up to a negative value. This indicates that it has a problem of transferring the electrons from the NSQN compound to the metal (110) surface.

3.6.1.3. *Local centers derived from conceptual DFT*

3.6.1.3.1. MESP distribution. Figure 14 shows the representations of molecular electrostatic potentials (*MESP*), i.e. the total electron density maps the molecular geometry of NSQN & CSQN. This representation of total density is described by the distribution of colors on selective regions such as positive regions (blue colors) and negative regions (red colors). Figure 14 shows that the comparison of the electron density of the strong region (red color) and weak (blue color) for the two inhibitors shows almost the same distribution of this density. Indeed, NSQN & CSQN have a delocalized negative region on the N7 and N10 nitrogen atoms, which increases the interactions with the metal surface. While the negative regions are located on the O12 atom. In addition, the same remark was observed for the protonated forms, knowing that the molecular surface for NSQN & CSQN is positively charged. This indicates that inhibitor/metal electrostatic interactions will be established.

3.6.1.3.2. Mulliken charges and Fukui indices. It is necessary to determine the active centers donor and acceptor of a molecule, for this we will detect these sites utilizing the atomic charges of Mulliken and the Fukui indices. The results of different electrophilic and nucleophilic sites of the NSQN & CSQN protonated and non-protonated molecules are grouped in the following Table 9. The values of the Mulliken charges distributed in Table 9 are negative and positive, reflecting the fact that the NSQN & CSQN molecules have active sites (donor-acceptor) that promote the responsiveness of these species with the iron atoms of M-steel. We noticed that the trend of all the values of the sites of protonated molecules is reduced remarkably, which indicates that molecular reactivity of protonated inhibitors is decreased, therefore, this result reflects the receiving character of protonated molecules [49]. Regarding the total negative charge (CNT), the same behavior was observed based on the results obtained in Table 9 and represented in Figure 15, whereas TNC was decreased after protonation of NSQN & CSQN [50]. This indicates that the structural reactivity of the protonated molecules is lowered. The TNC shows that NSQN has a higher electron donor property than CSQN. This promotes its adsorption capacity on the metal surface. These results are consistent with those found in the experimental part.

In acidic media (HCl), organic molecules with one or more heteroatoms are able to protonate at these sites, which leads to the formation of positively charged molecules. These interact with the anions that are well distributed (Cl^-) on the metal surface. In this context, we will follow this theory to see the effect of protonation on local centers belonging to inhibitory molecules. So, the third indicator such as Fukui's index (FI), the atoms of the studied molecules having higher values of f_k^- and f_k^- in the protonated and non-protonated form are represented in Figure 16. The overall analysis of this figure shows that each molecule is characterized by the same atoms for both forms studied either for electrophilic or nucleophilic attack. In general, we note that after protonation, the values of the atoms of f_k^- and f_k^- are decreased with exceptions of a few atoms in both forms. The results visualized in Figure 16 shows that after protonation donor property of nitrogen atoms (N10 and N31) have been decreased because these atoms are protonated, implying that these centers are blocked by protons H^+ [51].

If we take for example the NSQN compound that the highest values of f_k^- are the C (9), N (10), O (12) and C (13) atoms for both protonated and non-protonated forms, we also note after protonation, a decrease for the N (10) and O (12) atoms and an increase for the C (9) and C (13) atoms, These atoms participate in the acceptance of electrons from the metal surface. On the other hand, the C (11), C (14), C (18) and N (31) atoms

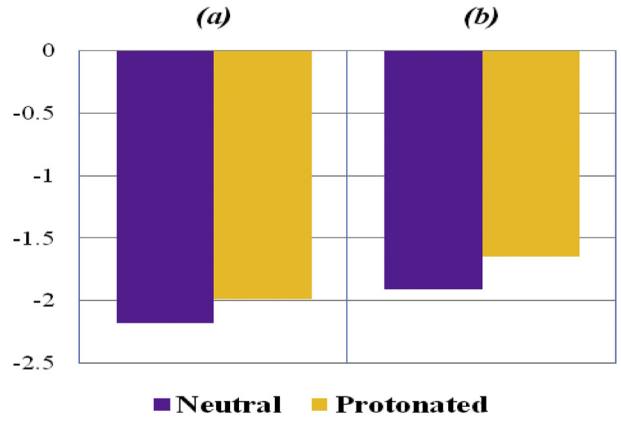

Figure 15. TNC of the NSQN (a) and CSQN (b) protonated and non-protonated molecules.

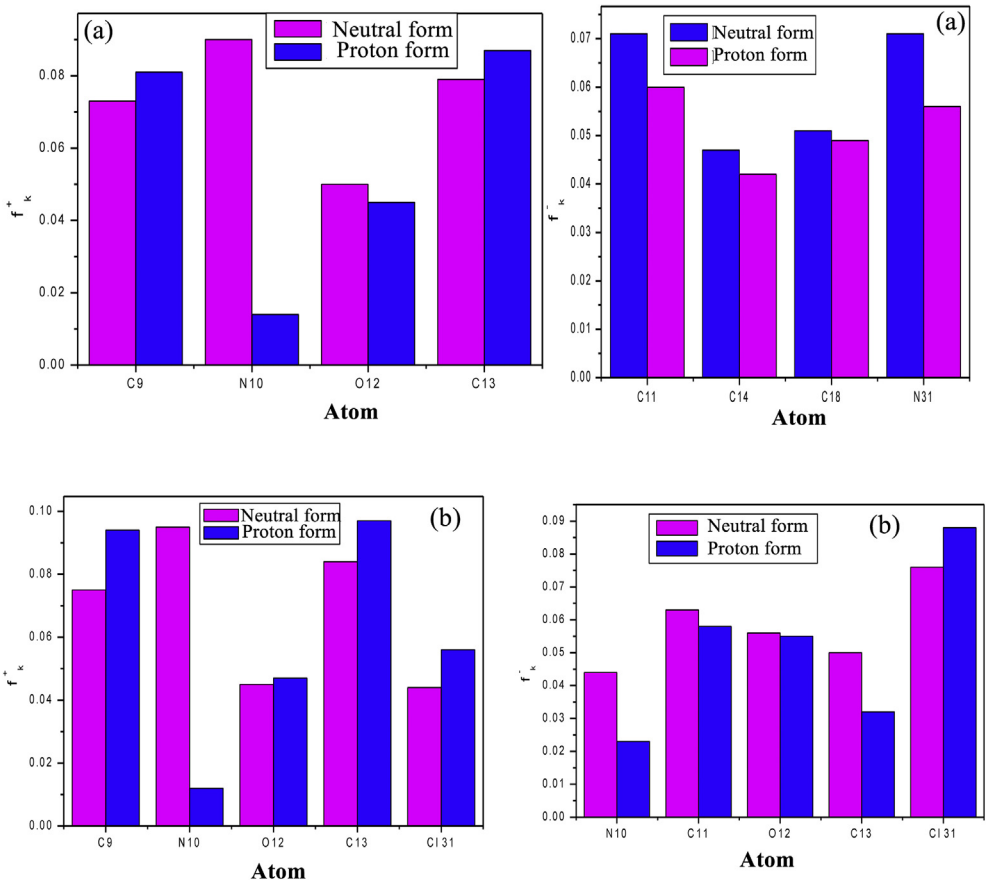

Figure 16. Graphical representation of the Fukui indices of NSQN(a) and CSQN(b) for the more reactive atoms in the unprotonated and protonated form.

are electron donors such that these atoms have higher f_k^- values.All the evolutions of the major atoms are represented in Figure 16.

3.6.2. Study of the interaction of NSQN & CSQN with the Fe (110) surface by molecular dynamics (MD) simulation

The complexity of the corrosion protection system necessitates considering the maximum of the factors involved in this process, such as the interaction energy (E_{ads}) between the elements of the system. From this effect and in order to complete the conclusions deduced from quantum computation (DFT/B3LYP). In this section, we are interested in exploring the interaction of NSQN & CSQN and the Fe (110) surface in a solution contains 500 water molecules. Recently, much attention has been devoted to the use of MD as a less expensive simulation tool in terms of computation time (in the aqueous phase), firstly, to quantify the interaction energy between the molecule of inhibitor and metal surface, and secondly, to find the most stable adsorption configuration (favorable adsorption sites).

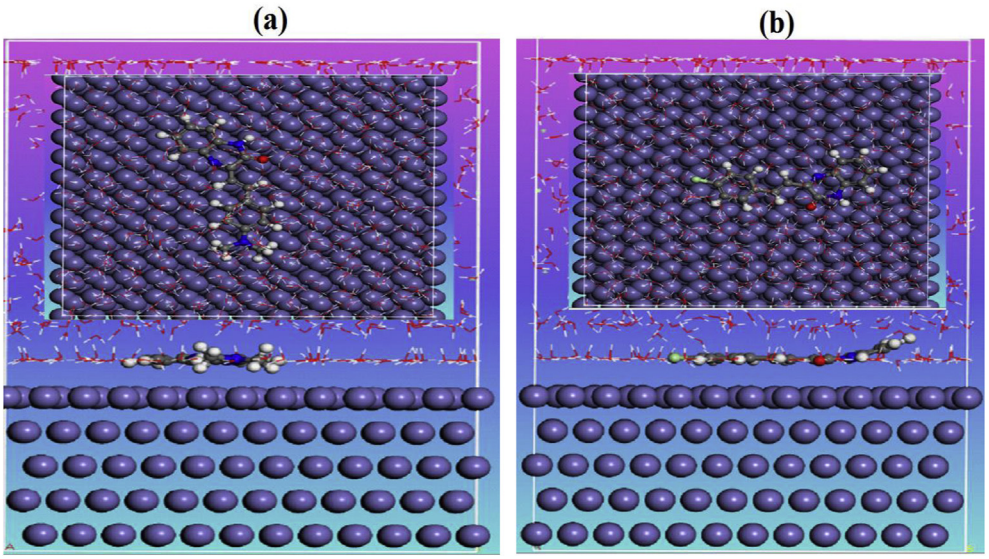

Figure 17. Most stable adsorption configuration of NSQN (a) and CSQN (b) chemical species (Top view).

Table 10. The adsorption energy of quinoxalines on the aqueous phase metal substrate (Fe (110)) in aqueous phase.

Investigated system	$E_{interaction}$ (kJ/mol)	$E_{binding}$ (kJ/mol)
NSQN + Fe (110)	-903.7	903.7
CSQN + Fe (110)	-768.3	768.3

In order to explore the solvent effect on the adsorption process of NSQN & CSQN on the surface of M-steel, the molecular dynamics simulation was carried out in aqueous phase (500 H_2O molecules). Reasonably, the MD simulation predicts the most favorable configuration of the adsorbed inhibitor on the M-steel, (when the adsorption process has reached equilibration) [52]. Figure 17 shows the most stable configuration of the system under study ((NSQN & CSQN) derived of quinoxaline +500 H_2O/Fe (110)) obtained at the end of the MD optimization process. As can be seen in this figure, NSQN & CSQN take a location just above the surface, which reflects the ability of these molecules to interact easily with the metal surface of M-steel (Fe (110)) in the presence of 500 H_2O. The presence of water molecules can lead to competition during the adsorption of quinoxalines on the surface of M-steel. This is remarkable in that the adsorption density distribution shows that the water molecules are more likely to adsorb to the M-steel surface.

The values of the binding ($E_{binding}$) and interaction ($E_{interaction}$) energies are arranged in Table 10. Analysis of the this tableau shows that the two derivatives of NSQN & CSQN have ability to adsorb on the surface of M-steel in the aqueous phase where $E_{interaction}$ calculated values are -768.3 kJ/mol for CSQN and -903.7 kJ/mol for NSQN. In addition, the negative sign indicates that this adsorption process is exothermic in nature [53]. The highest value of the $E_{interaction}$ for NSQN suggests that it is the best adsorption system and the most stable among the quinoxaline derivatives studied and therefore illustrates its high efficiency of corrosion inhibition. it can be deduced that the results obtained the theoretical study and the experimental study are in agreement [38].

4. Conclusions

The new quinoxaline compounds, namely 3-(4-(dimethylamino) quinoxalin-2(1*H*)-one (NSQN) and 3-(4-chlorostyryl)quinoxalin-2(1H)-one (CSQN) was investigated as corrosion inhibitors for M-steel in 1 M HCl medium at 303 K utilizing weight loss, electrochemical and surface techniques. These heterocyclic derivatives showed excellent inhibition performance. A good agreement was observed between the obtained values from the weight loss, polarization, and EIS techniques. The value of the inhibitory efficacy increases with the concentration of the examined compounds. Analysis of the polarization curves shows that the various compounds have a mixed character. Scanning electron microscopy analysis shows the formation of a protective layer that covers the surface of the metal. Theoretical calculations show that molecules with a high dipole moment and a high HOMO energy has a good inhibitory efficiency. Molecular dynamics simulations show the great interaction between the considered inhibitors and the metal surface.

Declarations

Author contribution statement

Abdelkader Zarrouk, Y. Ramli, A. Guenbour, I. Warad: Analyzed and interpreted the data; Contributed reagents, materials, analysis tools or data; Wrote the paper.

T. Laabaissi, F. Benhiba, M. Missioui, Z. Rouifi, M. Rbaa: Conceived and designed the experiments; Performed the experiments.

H. Oudda: Analyzed and interpreted the data; Contributed reagents, materials, analysis tools or data.

Funding statement

This research did not receive any specific grant from funding agencies in the public, commercial, or not-for-profit sectors.

Competing interest statement

The authors declare no conflict of interest.

Additional information

No additional information is available for this paper.

References

[1] D.D.N. Singh, T.B. Singh, B. Gaur, The role of metal cations in improving the inhibitive performance of hexamine on the corrosion of steel in hydrochloric acid solution, Corrosion Sci. 37 (1995) 1005–1019.
[2] G. Schmitt, Application of inhibitors for acid media: report prepared for the European federation of corrosion working party on inhibitors, Br. Corrosion J. 19 (1984) 165–176.
[3] A. Agrawal, K.K. Sahu, An overview of the recovery of acid from spent acidic solutions from steel and electroplating industries, J. Hazard Mater. 171 (2009) 61–75.
[4] A. Zarrouk, H. Zarrok, Y. Ramli, M. Bouachrine, B. Hammouti, A. Sahibed-dine, F. Bentiss, Inhibitive properties, adsorption and theoretical study of 3,7-dimethyl-1-(prop-2-yn-1-yl)quinoxalin-2(1H)-one as efficient corrosion inhibitor for carbon steel in hydrochloric acid solution, J. Mol. Liq. 222 (2016) 239–252.
[5] M. El Hezzat, M. Assouag, H. Zarrok, Z. Benzekri, A. El Assyry, S. Boukhris, A. Souizi, M. Galai, R. Touir, M. Ebn Touhami, H. Oudda, A. Zarrouk, Correlated DFT and electrochemical study on inhibition behavior of ethyl 6-amino-5-cyano-2-methyl-4-(p-tolyl)-4H-pyran-3-carboxylate for the corrosion of Mild steel in HCl, Der Pharma Chem. 7 (10) (2015) 77–88.
[6] M. El Faydy, M. Galai, A. El Assyry, A. Tazouti, R. Touir, B. Lakhrissi, M. Ebn Touhami, A. Zarrouk, Experimental investigation on the corrosion inhibition of carbon steel by 5-(chloromethyl)-8-quinolinol hydrochloride in hydrochloric acid solution, J. Mol. Liq. 219 (2016) 396–404.
[7] Y. ELouadi, F. Abrigach, A. Bouyanzer, R. Touzani, O. Riant, B. ElMahi, A. El Assyry, S. Radi, A. Zarrouk, B. Hammouti, Corrosion inhibition of Mild steel by new N-heterocyclic compound in 1 M HCl: experimental and computational study, Der Pharma Chem. 7 (8) (2015) 265–275.
[8] H. Zarrok, S.S. Al-Deyab, A. Zarrouk, R. Salghi, B. Hammouti, H. Oudda, M. Bouachrine, F. Bentiss, Thermodynamic characterisation and density functional theory investigation of 1, 1',5 , 5'-Tetramethyl-1H, 1'H-3, 3'- bipyrazole as corrosion inhibitor of C38 steel corrosion in HCl, Int. J. Electrochem. Sci. 7 (2012) 4047–4063.
[9] M.E. Faydy, M. Rbaa, L. Lakhrissi, B. Lakhrissi, I. Warad, A. Zarrouk, I.B. Obot, Corrosion protection of carbon steel by two newly synthesized benzimidazol-2-ones substituted 8-hydroxyquinoline derivatives in 1 M HCl: experimental and theoretical study, Surf. Interfaces 14 (2019) 222–237.
[10] Z. Salarvand, M. Amirnasr, M. Talebian, K. Raeissi, S. Meghdadi, Enhanced corrosion resistance of M-steel in 1 M HCl solution by trace amount of 2-phenyl-benzothiazole derivatives: experimental, quantum chemical calculations and molecular dynamics (MD) simulation studies, Corrosion Sci. 114 (2017) 133–145.
[11] S. Kaya, B. Tüzün, C. Kaya, I.B. Obot, Determination of corrosion inhibition effects of amino acids: quantum chemical and molecular dynamic simulation study, J. Taiwan Inst. Chem. Eng. 58 (2016) 528–535.
[12] P. Dohare, K.R. Ansari, M.A. Quraishi, I.B. Obot, Pyranpyrazole derivatives as novel corrosion inhibitors for M-steel useful for industrial pickling process: experimental and Quantum Chemical study, J. Ind. Eng. Chem. 52 (2017) 197–210.
[13] M. Saraçoğlu, M.I.A. Elusta, S. Kaya, C. Kaya, F. Kandemirli, Quantum chemical studies on the corrosion inhibition of Fe78B13Si9 glassy alloy in Na_2SO_4 solution of some thiosemicarbazone derivatives, Int. J. Electrochem. Sci. 13 (2018) 8241–8259.
[14] F. Tezcan, G. Yerlikaya, A. Mahmood, G. Kardaş, A novel thiophene Schiff base as an efficient corrosion inhibitor for M-steel in 1.0 M HCl: electrochemical and quantum chemical studies, J. Mol. Liq. 269 (2018) 398–406.
[15] S.K. Saha, M. Murmu, N.C. Murmu, I.B. Obot, P. Banerjee, Molecular level insights for the corrosion inhibition effectiveness of three amine derivatives on the carbon steel surface in the adverse medium: a combined density functional theory and molecular dynamics simulation study, Surf. Interfaces 10 (2018) 65–73.
[16] N. Boon, Efficient configurational-bias Monte-Carlo simulations of chain molecules with “swarms” of trial configurations, J. Chem. Phys. 149 (2018), 064109.
[17] D. Ben Hmamou, R. Salghi, A. Zarrouk, H. Zarrok, R. Touzani, B. Hammouti, A. El Assyry, Investigation of corrosion inhibition of carbon steel in 0.5 M H_2SO_4 by new bipyrazole derivative using experimental and theoretical approaches, J. Environ. Chem. Eng. 3 (2015) 2031–2041.
[18] N. Anusuya, J. Saranya, P. Sounthari, A. Zarrouk, S. Chitra, Corrosion inhibition and adsorption behaviour of some bis-pyrimidine derivatives on Mild steel in acidic medium, J. Mol. Liq. 225 (2017) 406–417.
[19] B. Xu, W. Yang, Y. Liu, X. Yin, W. Gong, Y. Chen, Experimental and theoretical evaluation of two pyridinecarboxaldehyde thiosemicarbazone compounds as

corrosion inhibitors for M-steel in hydrochloric acid solution, Corrosion Sci. 78 (2014) 260–268.
[20] N.V. Likhanova, M.A. Domínguez-Aguilar, O. Olivares-Xometl, N. Nava-Entzana, E. Arce, H. Dorantes, The effect of ionic liquids with imidazolium and pyridinium cations on the corrosion inhibition of M-steel in acidic environment, Corrosion Sci. 52 (2010) 2088–2097.
[21] M. El Faydy, R. Touir, M.E. Touhami, A. Zarrouk, C. Jama, B. Lakhrissi, L.O. Olasunkanmi, E.E. Ebenso, F. Bentiss, Corrosion inhibition performance of newly synthesized 5-alkoxymethyl-8-hydroxyquinoline derivatives for carbon steel in 1 M HCl solution: experimental, DFT and Monte Carlo simulation studies, Phys. Chem. Chem. Phys. 30 (2018) 20167–20187.
[22] M. Hosseini, S.F. Mertens, M. Ghorbani, M.R. Arshadi, Asymmetrical Schiff bases as inhibitors of M-steel corrosion in sulphuric acid media, Mater. Chem. Phys. 78 (2003) 800–808.
[23] D.K. Yadav, D.S. Chauhan, I. Ahamad, M.A. Quraishi, Electrochemical behavior of steel/acid interface: adsorption and inhibition effect of oligomeric aniline, RSC Adv. 3 (2013) 632–646.
[24] M. Kissi, M. Bouklah, B. Hammouti, M. Benkaddour, Establishment of equivalent circuits from electrochemical impedance spectroscopy study of corrosion inhibition of steel by pyrazine in sulphuric acidic solution, Appl. Surf. Sci. 252 (2006) 4190–4197.
[25] M. Rbaa, F. Benhiba, I.B. Obot, H. Oudda, I. Warad, B. Lakhrissi, A. Zarrouk, Two new 8-hydroxyquinoline derivatives as an efficient corrosion inhibitors for Mild steel in hydrochloric acid: synthesis, electrochemical, surface morphological, UV–visible and theoretical studies, J. Mol. Liq. 276 (2019) 120–133.
[26] C. Verma, L.O. Olasunkanmi, E.E. Ebenso, M.A. Quraishi, I.B. Obot, Adsorption behavior of glucosamine-based, pyrimidine-fused heterocycles as green corrosion inhibitors for M-steel: experimental and theoretical studies, J. Phys. Chem. C 120 (2016) 11598–11611.
[27] R. Solmaz, G. Kardaş, M. Culha, B. Yazıcı, M. Erbil, Investigation of adsorption and inhibitive effect of 2-mercaptothiazoline on corrosion of M-steel in hydrochloric acid media, Electrochim. Acta 53 (2008) 5941–5952.
[28] M. Özcan, I. Dehri, M. Erbil, Organic sulphur-containing compounds as corrosion inhibitors for M-steel in acidic media: correlation between inhibition efficiency and chemical structure, Appl. Surf. Sci. 236 (2004) 155–164.
[29] G. Avci, Corrosion inhibition of indole-3-acetic acid on M-steel in 0.5 M HCl, Colloids Surf. A 317 (2008) 730–736.
[30] V. Srivastava, D.S. Chauhan, P.G. Joshi, V. Maruthapandian, A.A. Sorour, M.A. Quraishi, PEG-functionalized chitosan: a biological macromolecule as a novel CorrosionInhibitor, ChemistrySelect 3 (2018) 1990–1998.
[31] Y. EL Aoufir, H. Lgaz, H. Bourazmi, Y. Kerroum, Y. Ramli, A. Guenbour, R. Salghi, F. El-Hajjaji, B. Hammouti, H. Oudda, Quinoxaline derivatives as corrosion inhibitors of carbon steel in hydrochloridric acid media: electrochemical, DFT and Monte Carlo simulations studies, J. Mater. Environ. Sci. 7 (12) (2016) 4330–4347.
[32] S. Bahri, M. Belayachi, H. Zarok, A. Shaim, M. Galai, A. Zarrouk, A. El Midaoui, M. Ebn Touhami, B. Lakhrissi, H. Oudda, Electrochemical investigation of 6-methylquinoxaline-2,3(1H,4H)-dione as potential corrosion inhibitor for carbon steel in hydrochloric acid solution, Der Pharma Chem. 6 (3) (2014) 110–118.
[33] H. Tayebi, H. Bourazmi, B. Himmi, A. El Assyry, Y. Ramli, A. Zarrouk, A. Geunbour, B. Hammouti, Combined electrochemical and quantum chemical study of new quinoxaline derivative as corrosion inhibitor for carbon steel in acidic media, Der Pharma Chem. 6 (5) (2014) 220–234.
[34] T. Laabaissi, F. Benhiba, Z. Rouifi, M. Missioui, K. Ourrak, H. Oudda, Y. Ramli, I. Warad, M. Allali, A. Zarrouk, New quinoxaline derivative as a green corrosion inhibitor for Mild steel in mild acidic medium: electrochemical and theoretical studies, Int. J. Corros. Scale Inhib. 8 (2) (2019) 241–256.
[35] M. Benabdellah, A. Tounsi, K.F. Khaled, B. Hammouti, Thermodynamic, chemical and electrochemical investigations of 2-mercapto benzimidazole as corrosion inhibitor for M-steel in hydrochloric acid solutions, Arab. J. Chem. 4 (2011) 17–24.
[36] K. Ansari, M. Quraishi, A. Singh, Schiff's base of pyridyl substituted triazoles as new and effective corrosion inhibitors for M-steel in hydrochloric acid solution, Corrosion Sci. 79 (2014) 5–15.
[37] M. El Azzouzi, A. Aouniti, S. Tighadouin, H. Elmsellem, S. Radi, B. Hammouti, A. El Assyry, F. Bentiss, A. Zarrouk, Some hydrazine derivatives as corrosion inhibitors for Mild steel in 1.0 M HCl: weight loss, electrochemichal, SEM and theoretical studies, J. Mol. Liq. 221 (2016) 633–641.
[38] A. Salhi, S. Tighadouini, M. El-Massaoudi, M. Elbelghiti, A. Bouyanzer, S. Radi, S. El Barkany, F. Bentiss, A. Zarrouk, Keto-enol heterocycles as new compounds of corrosion inhibitors for carbon steel in 1 M HCl: weight loss, electrochemical and quantum chemical investigation, J. Mol. Liq. 248 (2017) 340–349.
[39] M. Mobin, M. Rizvi, Polysaccharide from *Plantago* as a green corrosion inhibitor for carbon steel in 1 M HCl solution, Carbohydr. Polym. 160 (2017) 172–183.
[40] Y. Sangeetha, S. Meenakshi, C. Sairam Sundaram, Corrosion inhibition of aminated hydroxyl ethyl cellulose on M-steel in acidic condition, Carbohydr. Polym. 150 (2016) 13–20.
[41] M.A. Deyab, Inhibition activity of Seaweed extract for mild carbon steel corrosion in saline formation water, Desalination 384 (2016) 60–67.
[42] R.L. Camacho-Mendoza, E. Gutiérrez-Moreno, E. Guzmán-Percástegui, E. Aquino-Torres, J. Cruz-Borbolla, J.A. Rodríguez-Ávila, J.G. Alvarado-Rodríguez, O. Olvera-Neria, P. Thangarasu, J.L. Medina-Franco, Density functional theory and electrochemical studies: structure-efficiency relationship on corrosion inhibition, J. Chem. Inf. Model. 55 (2015) 2391–2402.
[43] B. Thapa, H.B. Schlegel, Density functional theory calculation of pKa's of Thiols in aqueous solution using explicit water molecules and the polarizable continuum model, J. Phys. Chem. A 120 (2016) 5726–5735.
[44] D. Bellinger, V. Settels, W. Liu, R.F. Fink, B. Engels, Influence of a polarizable surrounding on the electronically excited states of aggregated perylene materials, J. Comput. Chem. 37 (2016) 1601–1610.
[45] Ş. Erdoğan, Z.S. Safi, S. Kaya, D.Ö. Işın, L. Guo, C. Kaya, A computational study on corrosion inhibition performances of novel quinoline derivatives against the corrosion of iron, J. Mol. Struct. 1134 (2017) 751–761.
[46] J. Frau, D. Glossman-Mitnik, Chemical reactivity theory applied to the calculation of the local reactivity descriptors of a colored maillard reaction, Product. Chem. Sci. Int. J. 22 (2018) 1–14.
[47] P. Dohare, D.S. Chauhan, A.A. Sorour, M.A. Quraishi, DFT and experimental studies on the inhibition potentials of expired Tramadol drug on Mild steel corrosion in hydrochloric acid, Mater. Discover. 9 (2017) 30–41.
[48] H. Sheng, H. Zhang, W. Song, H. Ji, W. Ma, C. Chen, J. Zhao, Activation of water in titanium dioxide photocatalysis by formation of surface hydrogen bonds: an in situ IR spectroscopy study, Angew. Chem. Int. Ed. 54 (2015) 5905–5909.
[49] S.K. Saha, A. Hens, N.C. Murmu, P. Banerjee, A comparative density functional theory and molecular dynamics simulation studies of the corrosion inhibitory action of two novel N-heterocyclic organic compounds along with a few others over steel surface, J. Mol. Liq. 215 (2016) 486–495.
[50] J. Bonin, A. Maurin, M. Robert, Molecular catalysis of the electrochemical and photochemical reduction of CO_2 with Fe and Co metal based complexes, Recent Adv. Coord. Chem. Rev. 334 (2017) 184–198.
[51] N.O. Obi-Egbedi, I.B. Obot, A.O. Eseola, Synthesis, characterization and corrosion inhibition efficiency of 2-(6-methylpyridin-2-yl)-1H-imidazo[4,5-f][1,10] phenanthroline on M-steel in sulphuric acid, Arab. J. Chem. 7 (2014) 197–207.
[52] G. Olivieri, K.M. Parry, R. D'Auria, D.J. Tobias, M.A. Brown, Specific anion effects on Na^+ adsorption at the aqueous solution–air interface: MD simulations, SESSA calculations, and photoelectron spectroscopy experiments, J. Phys. Chem. B 122 (2018) 910–918.
[53] S.K. Saha, M. Murmu, N.C. Murmu, P. Banerjee, Evaluating electronic structure of quinazolinone and pyrimidinone molecules for its corrosion inhibition effectiveness on target specific Mild steel in the acidic medium: a combined DFT and MD simulation study, J. Mol. Liq. 224 (2016) 629–638.